

# Oriented Triplet $p$ -Wave Pairing from Fermi surface Anisotropy and Nonlocal Attraction

Shuning Tan,<sup>1,\*</sup> Ji Liu,<sup>2,3,\*</sup> Minghuan Zeng,<sup>4</sup> Tao Ying,<sup>5</sup> Zhangkai Cao,<sup>6,7,†</sup> and Ho-Kin Tang<sup>2,3,‡</sup>

<sup>1</sup>*Key Laboratory for Microstructural Material Physics of Hebei Province,  
School of Science, Yanshan University, Qinhuangdao 066004, China*

<sup>2</sup>*School of Science, Harbin Institute of Technology, Shenzhen, 518055, China*

<sup>3</sup>*Shenzhen Key Laboratory of Advanced Functional Carbon Materials  
Research and Comprehensive Application, Shenzhen 518055, China.*

<sup>4</sup>*College of Physics, Chongqing University, Chongqing 401331, China*

<sup>5</sup>*School of Physics, Harbin Institute of Technology, Harbin 150001, China*

<sup>6</sup>*Eastern Institute for Advanced Study, Eastern Institute of Technology, Ningbo, Zhejiang 315200, China*

<sup>7</sup>*School of Physical Sciences, University of Science and Technology of China, Hefei, 230026, China*

(Dated: January 19, 2026)

Using constrained-path quantum Monte Carlo, we map the ground-state phase diagram versus the nearest-neighbor (NN) attraction  $V$  and spin-dependent hopping anisotropy  $\alpha$  for the two-dimensional attractive  $t$ - $U$ - $V$  Hubbard model at filling  $n \simeq 0.85$ . We identify an onsite  $s$ -wave superfluid, a Cooper pair Bose metal with an uncondensed Bose surface, and an oriented equal-spin triplet  $p$ -wave pairing phase. The NN attraction activates the odd-parity channel, while hopping anisotropy suppresses the competing  $s$ -wave coherence and selects a  $p_x/p_y$  polar axis, and thus lowers the critical  $|V_c|$  for the onset of triplet-dominant  $p$ -wave pairing. A channel-resolved Landau analysis provides a criterion for the Landau  $p$ -wave scale  $V_c^L(\alpha)$ , consistent with the observed anisotropy dependence of  $|V_c|$ . Our results establish how NN interaction and Fermi surface anisotropy cooperate to generate the oriented triplet  $p$ -wave pairing, and suggest that cold-atom and altermagnetic platforms could potentially realize this mechanism.

Spin-triplet  $p$ -wave pairing has long been pursued as a route to odd-parity superconductivity and topological superfluids hosting Majorana modes [1–7]. Yet in microscopic lattice settings it is typically fragile: on-site attraction strongly favors singlet  $s$ -wave pairing and readily preempts odd-parity channels [8–15]. A key challenge is therefore to identify a minimal, controllable mechanism that both weakens the competing singlet channel and stabilizes an oriented triplet  $p$ -wave tendency, ideally in ultracold-atom optical lattices where state-dependent tunneling and the interaction range can be engineered with high precision [16–20].

Two ingredients naturally address this challenge. First, spin-dependent hopping anisotropy deforms the spin-resolved Fermi surface and suppresses conventional on-site  $s$ -wave coherence, opening phase space for unconventional pairing [21, 22]. Such Fermi surface geometry can also organize pairing correlations into a Cooper-pair Bose metal (CPBM), a gapless paired regime with a momentum-space “Bose surface” but without superfluid stiffness [21, 23–25]. Second, a finite-range attraction—here taken as the nearest-neighbor (NN) attraction ( $V < 0$ )—directly activates symmetry-allowed odd-parity channels and enhances triplet pairing tendencies once singlet pairing is weakened [26–28]. However, how spin-dependent Fermi surface deformation and NN attraction cooperate to reshape both the strength and

the orientation of the leading pairing correlations in a controlled lattice setting remains an open question.

In this work, we carry out constrained-path quantum Monte Carlo (CPQMC) simulations [29, 30] to study the attractive two-dimensional  $t$ - $U$ - $V$  Hubbard model with the spin-dependent anisotropic hopping. At filling  $n \simeq 0.85$ , we map the ground-state phase diagram in the  $(V, \alpha)$  plane, where  $V$  denotes the NN attraction and  $\alpha$  parameterizes the spin-dependent hopping anisotropy. We identify three regimes: an onsite  $s$ -wave superfluid ( $s$ -SF), a CPBM, and an oriented spin-triplet  $p$ -wave pairing ( $p$ -TP) that appears for finite NN attraction strengths. Increasing the spin anisotropy suppresses the competing onsite  $s$ -wave channel and lowers the critical strength  $|V_c(\alpha)|$  at which the  $p$ -wave vertex becomes dominant over the  $s$ -wave. Momentum-resolved bubble-subtracted pairing correlators resolve an uncondensed Bose surface in the CPBM and a  $\Gamma$ -centered, anisotropically elongated triplet vertex enhancement whose polar axis tracks the spin-resolved Fermi surface patches. A channel-resolved Landau analysis provides a compact rationalization and yields a simple criterion for Landau scale  $V_c^L(\alpha)$ , whose anisotropy dependence tracks the numerical trend of  $V_c(\alpha)$ .

\* These authors contributed equally.

† caozhangkai@mail.bnu.edu.cn

‡ denghaojian@hit.edu.cn

Motivated by cold-atom realizations of attractive Hubbard-type models with tunable interaction range [31–35], we study the two-dimensional attractive  $t$ - $U$ - $V$  Hubbard model on a square lattice with spin-

dependent anisotropic hopping,

$$H = - \sum_{i,\sigma,\delta} t_{\delta,\sigma} (\hat{c}_{i,\sigma}^\dagger \hat{c}_{i+\delta,\sigma} + \text{h.c.}) + U \sum_i \hat{n}_{i\uparrow} \hat{n}_{i\downarrow} + V \sum_{i,\delta,\sigma,\sigma'} \hat{n}_{i,\sigma} \hat{n}_{i+\delta,\sigma'}. \quad (1)$$

Here  $\hat{c}_{i\sigma}^\dagger$  ( $\hat{c}_{i\sigma}$ ) creates (annihilates) a fermion with spin  $\sigma = \uparrow, \downarrow$  on site  $i$ , and  $\hat{n}_{i\sigma} = \hat{c}_{i\sigma}^\dagger \hat{c}_{i\sigma}$  is the electron number operator. The hopping amplitude is  $t_{\delta,\sigma}$ , where the displacement  $\delta \in \{\hat{x}, \hat{y}\}$  connects site  $i$  to its NN  $i + \delta$ . Unless otherwise specified, we set  $t \equiv 1$  and work at filling  $n \simeq 0.85$  with  $U = -3$ .

In addition to onsite attraction  $U < 0$ , we include a NN attraction  $V < 0$  as the minimal short-range extension that captures the competition between conventional onsite singlet pairing and odd-parity pairing allowed by symmetry on the square lattice. As illustrated in the inset of Fig. 1, we choose spin-dependent anisotropic NN hoppings  $t_{\hat{y},\downarrow} = t_{\hat{x},\uparrow} = t$  and  $t_{\hat{x},\downarrow} = t_{\hat{y},\uparrow} = \alpha t$ , and tune  $\alpha \in [0, 1]$  from the isotropic ( $C_4$ -symmetric) limit  $\alpha = 1$  to the quasi-one-dimensional limit  $\alpha = 0$ ; the hopping pattern is invariant under a  $\pi/2$  lattice rotation followed by exchanging  $\uparrow$  and  $\downarrow$ . We work at zero spin polarization,  $\langle \hat{n}_{i\uparrow} \rangle = \langle \hat{n}_{i\downarrow} \rangle = n/2$ . In this setting,  $U$  favors onsite  $s$ -wave singlet correlations, whereas the finite-range attraction  $V$  activates odd-parity  $p$ -wave channels. For the spin-resolved Fermi-surface geometries relevant here, other even-parity NN form factors (extended- $s'$  and  $d_{x^2-y^2}$ ) remain subleading (see Supplemental Material [36]); accordingly, we focus on the dominant  $s$ - and  $p$ -wave channels.

To diagnose these dominant pairing channels, we introduce the corresponding equal-time pair operators: an onsite singlet,  $\Delta_s(i) = c_{i\downarrow} c_{i\uparrow}$  and NN equal-spin triplets,  $\Delta_{p_\eta,\sigma}(i) = \sum_{\delta \in \text{NN}} f_\delta^{(\eta)} c_{i+\delta,\sigma} c_{i\sigma}$ , with  $\eta \in \{x, y\}$  and  $\sigma \in \{\uparrow, \downarrow\}$ . The odd-parity form factors are subjected to the relation,  $f_{+\hat{x}/\hat{y}}^{(x/y)} = +1$  and  $f_{-\hat{x}/\hat{y}}^{(x/y)} = -1$ , and vanish otherwise. We also define the equal-time single-particle Green's functions  $G_{ij}^\sigma \equiv \langle c_{i\sigma}^\dagger c_{j\sigma} \rangle$ .

Following the bubble-subtracted (vertex) definition used in Ref. [28] (see also Refs. [25, 37, 38]), we remove the uncorrelated background built from one-body propagators and define the effective pair correlators as

$$C_s^{\text{eff}}(i, j) = \langle \Delta_s^\dagger(i) \Delta_s(j) \rangle - G_{i,j}^\uparrow G_{i,j}^\downarrow, \quad (2)$$

$$C_{p,\sigma}^{(\eta)}(i, j) = \langle \Delta_{p_\eta,\sigma}^\dagger(i) \Delta_{p_\eta,\sigma}(j) \rangle - \Lambda_{p,\sigma}^{(\eta)}(i, j). \quad (3)$$

with the bubble term

$$\Lambda_{p,\sigma}^{(\eta)}(i, j) = \sum_{\delta, \delta' \in \text{NN}} f_\delta^{(\eta)} f_{\delta'}^{(\eta)} G_{i,j}^\sigma G_{i+\delta,j+\delta'}^\sigma. \quad (4)$$

This subtraction isolates the interaction-driven vertex contribution in the Cooper channel, so the effective vertex highlights the interaction-induced vertex enhancement in the Cooper channel that signals pairing. Finally,

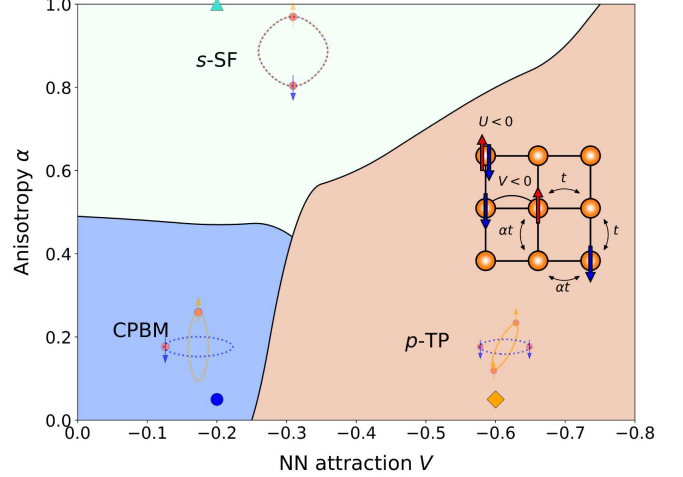


FIG. 1. (Color online) Ground-state phase diagram of the spin-anisotropic attractive  $t$ - $U$ - $V$  Hubbard model [Eq. (1).] at  $U = -3$  (with  $t = 1$ ) and filling  $n \simeq 0.85$ , estimated from quantum Monte Carlo simulations. The horizontal axis is the nearest-neighbor attractive interaction  $V$ , and the vertical axis is the hopping anisotropy parameter  $\alpha$ . We identify an onsite  $s$ -wave superfluid ( $s$ -SF), a Cooper pair Bose metal (CPBM), and an oriented spin-triplet  $p$ -wave pairing phase ( $p$ -TP). Decreasing  $\alpha$  suppresses  $s$ -wave coherence and drives the system into the CPBM regime at small  $|V|$ , while a sufficiently strong NN attraction,  $|V| > |V_c(\alpha)|$ , stabilizes the  $p$ -TP. Inset: spin-dependent hoppings  $t_{x\uparrow} = t_{y\downarrow} = t$  and  $t_{y\uparrow} = t_{x\downarrow} = \alpha t$ . Symbols denote representative data parameters in Fig. 3.

we obtain the pairing momentum-resolved vertex distributions via

$$N_\ell^{\text{eff}}(\mathbf{k}) = \frac{1}{N} \sum_{i,j} e^{i\mathbf{k} \cdot (\mathbf{r}_i - \mathbf{r}_j)} C_\ell^{\text{eff}}(i, j), \quad \ell \in \{s, (p_\eta, \sigma)\}, \quad (5)$$

where  $N$  is the number of sites. For the triplet sector we report the dominant channel,  $N_{p\text{-pair}}^{\text{eff}}(\mathbf{k}) \equiv \max_{\eta=x,y; \sigma=\uparrow,\downarrow} N_{p_\eta,\sigma}^{\text{eff}}(\mathbf{k})$ , and define its maximum value as  $N_{p\text{-pair}}^{\text{eff}}(\mathbf{k}_{\text{max}}) \equiv \max_{\mathbf{k}} N_{p\text{-pair}}^{\text{eff}}(\mathbf{k})$ , where  $\mathbf{k}_{\text{max}}$  denotes the momentum at which  $N_{p\text{-pair}}^{\text{eff}}(\mathbf{k})$  is maximized. Details of the CPQMC implementation and parameter settings can be found in Ref. [25].

Fig. 1 summarizes the ground-state phase diagram of the spin-anisotropic attractive  $t$ - $U$ - $V$  Hubbard model on square lattices up to  $20 \times 20$ . The phase diagram is presented in the  $(V, \alpha)$  plane, where phase boundaries are inferred from finite-size CPQMC data and serve as estimates for the thermodynamic limits. For weak anisotropy ( $\alpha \simeq 1$ ) and small  $|V|$ , the onsite attraction stabilizes  $s$ -SF. Upon decreasing  $\alpha$ , the spin-resolved Fermi surface deformation suppresses singlet coherence and eventually destroys the  $s$ -wave condensate, driving the system into the CPBM regime [21, 23–25, 39, 40]. At the vanishing NN attraction, we observe a crossover from  $s$ -SF to CPBM as  $\alpha$  is reduced, while no signature of a dominant  $p$ -TP instability is found within the anisotropy

range studied.

For  $V < 0$ , the NN attraction provides an odd-parity pairing channel, and an oriented  $p$ -TP emerges once  $|V|$  exceeds a critical value  $|V_c(\alpha)|$  where the dominant  $p$ -wave vertex weight overtakes the  $s$ -wave vertex weight. Stronger anisotropies reduce  $|V_c|$  by suppressing the competing onsite  $s$ -wave pairing correlations, thereby expanding the  $p$ -TP regime. In particular, at large spin anisotropies, the CPBM found at small  $|V|$  is replaced by the  $p$ -TP upon increasing  $|V|$ , highlighting how the spin anisotropy and nonlocal attraction cooperate to give rise to the  $p$ -TP: the spin anisotropy weakens  $s$ -wave coherence, while  $V$  provides the odd-parity  $p$ -wave channel.

We perform a minimal channel-resolved Landau analysis formulated in terms of normal-state Cooper bubbles [41–48]. Fourier transforming Eq. (1) yields the spin-dependent dispersions  $\xi_{\mathbf{k}\uparrow} = -2t(\cos k_x + \alpha \cos k_y) - \mu$  and  $\xi_{\mathbf{k}\downarrow} = -2t(\alpha \cos k_x + \cos k_y) - \mu$ , where  $\mu$  is fixed by the filling. The momentum-dependent kernel function from the onsite and NN interaction reads

$$V(\mathbf{k}, \mathbf{k}') = U + 2V[\cos(k_x - k'_x) + \cos(k_y - k'_y)]. \quad (6)$$

Projecting  $V(\mathbf{k}, \mathbf{k}')$  onto the symmetry-adapted basis  $\{1, \sin k_x, \sin k_y\}$  for onsite  $s$ -wave and NN equal-spin  $p$ -wave pairing, we obtain the channel couplings  $g_s = U$ ,  $g_{p_x} = g_{p_y} = 2V$ . The NN attraction also generates extended  $s'$  and  $d_{x^2-y^2}$  form factors, but their pairing susceptibilities are much smaller for Fermi surface geometries with spin anisotropy (see the Supplemental Material for details [36]). Integrating out the fermions and keeping only quadratic terms in the pairing fields yields the Landau coefficients

$$a_s(T, \alpha) = \frac{1}{|U|} - \Pi_s(T, \alpha), \quad (7)$$

$$a_{p_\eta, \sigma}(T, \alpha) = \frac{1}{2|V|} - \Pi_{p\eta, \sigma}(T, \alpha), \quad \eta = x, y, \sigma = \uparrow, \downarrow. \quad (8)$$

Here,  $\Pi_s$  and  $\Pi_{p\eta, \sigma}$  are the normal-state Cooper-channel susceptibilities (BCS bubbles) computed from the free Green's functions  $G_{0, \sigma}(\mathbf{k}, i\omega_n) = (i\omega_n - \xi_{\mathbf{k}\sigma})^{-1}$  with  $\omega_n = (2n + 1)\pi T$ . In practice, we evaluate these bubbles at low temperatures to reach the ground-state instabilities. Performing the Matsubara sum yields the explicit forms

$$\Pi_s(T, \alpha) = \frac{1}{N} \sum_{\mathbf{k}} \frac{\tanh(\xi_{\mathbf{k}\uparrow}/2T) + \tanh(\xi_{\mathbf{k}\downarrow}/2T)}{2(\xi_{\mathbf{k}\uparrow} + \xi_{\mathbf{k}\downarrow})}, \quad (9)$$

$$\Pi_{p\eta, \sigma}(T, \alpha) = \frac{1}{N} \sum_{\mathbf{k}} \sin^2 k_\eta \frac{\tanh(\xi_{\mathbf{k}\sigma}/2T)}{2\xi_{\mathbf{k}\sigma}}, \quad (10)$$

whose derivation and bubble diagrams are provided in the Supplemental Material [36].

Because  $\Pi_s$  involves both spin branches, decreasing  $\alpha$  reduces  $\Pi_s$  via Fermi surface mismatch and thus suppresses onsite  $s$ -wave coherence. In contrast,  $\Pi_{p\eta, \sigma}$  is an equal-spin bubble on a single branch weighted by the

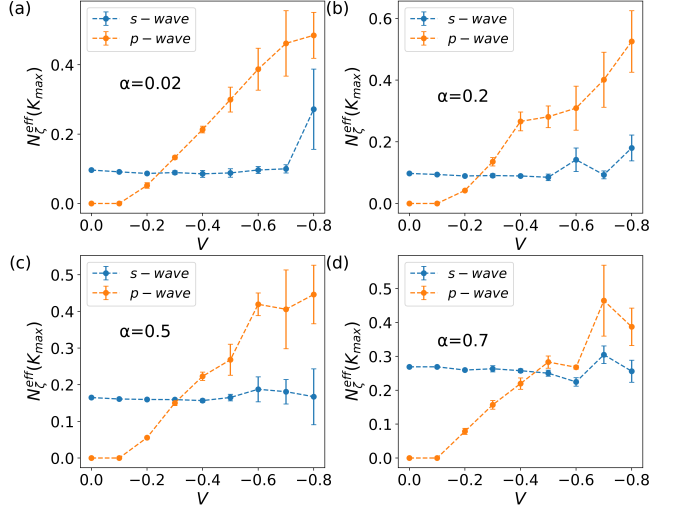


FIG. 2. (Color online) Maximum vertex weight  $N_\ell^{\text{eff}}(\mathbf{k}_{\text{max}})$  for the onsite  $s$ -wave (blue) and NN equal-spin  $p$ -wave (orange) channels versus NN attraction  $V$ . Panels (a)–(d) correspond to hopping anisotropy  $\alpha = 0.02, 0.2, 0.5$ , and  $0.7$ , respectively. The error bars denote statistical uncertainties.

odd-parity form factor  $\sin^2 k_\eta$ . Therefore, for each spin, anisotropy lifts the near-degeneracy between the  $p_x$  and  $p_y$  components and the dominant triplet sector is selected via  $\max_{\eta, \sigma} \Pi_{p\eta, \sigma}(T, \alpha)$ . At the Gaussian level, the Thouless condition  $a_{p\eta, \sigma}(T, \alpha) = 0$  defines a Landau scale for the onset of the leading triplet instability,

$$|V_c^L(\alpha)| = \left[ 2 \max_{\eta, \sigma} \Pi_{p\eta, \sigma}(T, \alpha) \right]^{-1}. \quad (11)$$

To compactly compare the pairing tendencies across channels, we summarize the momentum-resolved vertex distributions  $N_\ell^{\text{eff}}(\mathbf{k})$  by their maxima  $N_\ell^{\text{eff}}(\mathbf{k}_{\text{max}})$ . Fig. 2 shows  $N_s^{\text{eff}}(\mathbf{k}_{\text{max}})$  and the dominant NN equal-spin  $p$ -wave signal as functions of  $V$  for several anisotropies  $\alpha$ . For strong spin-dependent hopping anisotropy ( $\alpha = 0.02$ ),  $N_s^{\text{eff}}(\mathbf{k}_{\text{max}})$  depends only weakly on  $V$ , consistent with the onsite attraction  $U < 0$  controlling the singlet channel, whereas the  $p$ -wave vertex weight drops rapidly toward the noise floor as  $V \rightarrow 0^-$ . The crossing of the two curves provides an empirical estimate of the critical attraction  $V_c(\alpha)$  beyond which the  $p$ -wave vertex becomes dominant (e.g.,  $V_c(0.02) \simeq -0.23$ ). Upon increasing  $\alpha$  [Figs. 2(b)–2(d)], the crossing shifts systematically to more negative  $V$ , indicating that reduced anisotropy requires stronger NN attraction to stabilize dominant  $p$ -wave correlations. This trend mirrors the decrease of the Landau  $p$ -wave scale  $|V_c^L(\alpha)| = [2 \max_{\eta, \sigma} \Pi_{p\eta, \sigma}(T, \alpha)]^{-1}$  in Eq. (11).

Having established from Figs. 1 and 2 that the leading pairing channel switches between the  $s$ - and  $p$ -wave sectors as  $(V, \alpha)$  are tuned, we now examine momentum- and real-space signatures of the effective pairing correlations. In the CPBM [Fig. 3(a)],  $N_{s\text{-pair}}^{\text{eff}}(\mathbf{k})$  forms a broad, continuous nonzero momentum Bose surface, consistent

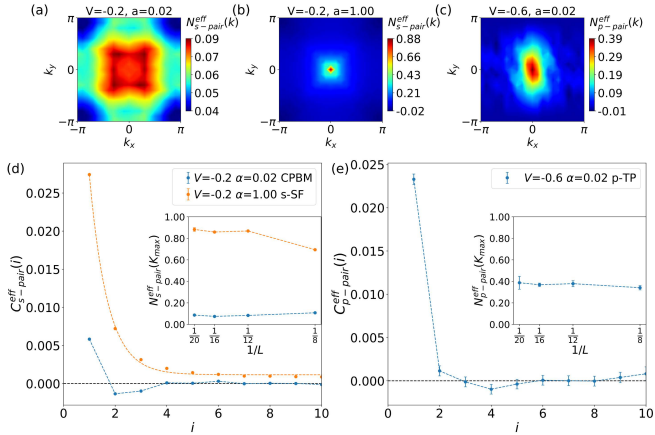


FIG. 3. (Color online) Pairing vertex distributions and correlators in the  $t-U-V$  model. Panels (a)–(c) correspond to the CPBM (circle),  $s$ -SF (triangle), and  $p$ -TP (diamond) points in Fig. 1: (a)  $N_{s\text{-pair}}^{\text{eff}}(\mathbf{k})$  at  $V = -0.2$ ,  $\alpha = 0.02$ ; (b)  $N_{s\text{-pair}}^{\text{eff}}(\mathbf{k})$  at  $V = -0.2$ ,  $\alpha = 1.00$ ; (c)  $N_{p\text{-pair}}^{\text{eff}}(\mathbf{k})$  at  $V = -0.6$ ,  $\alpha = 0.02$ . (d)  $C_{s\text{-pair}}^{\text{eff}}(i)$  for (a) and (b); inset: scaling of  $N_{s\text{-pair}}^{\text{eff}}(k_{\text{max}})$ . (e)  $C_{p\text{-pair}}^{\text{eff}}(i)$  for (c); inset: scaling of  $N_{p\text{-pair}}^{\text{eff}}(k_{\text{max}})$ .

with preformed yet uncondensed Cooper pairs and the absence of global phase coherence [21]. By contrast, in the  $s$ -SF [Fig. 3(b)] the distribution develops a sharp peak at  $\mathbf{k} = 0$ , signaling Bose condensation of Cooper pairs and long-range phase coherence. The real-space correlator  $C_{s\text{-pair}}^{\text{eff}}(i)$  [Fig. 3(d)] decays rapidly and oscillates about zero in the CPBM, but remains positive over much longer distances in the  $s$ -SF. Consistently, the inset shows that  $N_{s\text{-pair}}^{\text{eff}}(k_{\text{max}})$  extrapolates to a finite value in the  $s$ -SF, whereas in the CPBM it saturates with system size, consistent with the absence of off-diagonal long range order.

Now we focus on the  $p$ -TP regime and show the effective  $p$ -wave momentum distribution  $N_{p\text{-pair}}^{\text{eff}}(\mathbf{k})$  at strong anisotropy  $\alpha = 0.02$  and  $V = -0.6$ , as shown in Fig. 3(c). A pronounced lobe centered at  $\Gamma$  elongates along a single momentum axis, indicating a polar selection between the nearly degenerate  $p_x/p_y$  components. This oriented selection reflects the anisotropy-induced reshaping of the spin-resolved Fermi surface patches and the resulting lifting of the  $p_x-p_y$  near-degeneracy, consistent with our Landau analysis. In real-space [Fig. 3(e)],  $C_{p\text{-pair}}^{\text{eff}}(i)$  remains small and decays rapidly over accessible sizes, so establishing asymptotic off-diagonal long range order from  $C_{p\text{-pair}}^{\text{eff}}(r)$  alone is challenging. Nevertheless, the inset shows that the maximal vertex weight  $N_{p\text{-pair}}^{\text{eff}}(k_{\text{max}})$  remains appreciable and exhibits a weak but systematic size dependence, suggesting enhanced interaction-driven triplet pairing correlations in this regime.

To expose how the polar axis of the  $p$ -TP phase is selected microscopically, we next examine in Fig. 4 the full momentum-space evolution of the  $p$ -wave vertex distribution  $N_{p\text{-pair}}^{\text{eff}}(\mathbf{k})$  as a function of the NN attraction  $V$  and the hopping anisotropy  $\alpha$ . Panels 4(a)–4(d) show

a sequence of  $V$  at strong anisotropy  $\alpha = 0.02$ , while panels 4(f)–4(i) display the same  $V$  values at moderate anisotropy  $\alpha = 0.50$ . The rightmost panels 4(e) and 4(j) plot the corresponding spin-resolved Fermi surface, highlighting how spin-dependent hopping reshapes the spin-split Fermi surface patches. Because  $N_{p\text{-pair}}^{\text{eff}}(\mathbf{k})$  is bubble-subtracted, it fluctuates around zero ( $p$ -wave pairing is entirely absent) when  $V = 0$ , providing a clean baseline for isolating interaction-induced vertex enhancement.

At fixed  $\alpha$ , increasing  $|V|$  immediately generates a pronounced odd-parity vertex contribution concentrated near  $\Gamma$ , and the overall scale of  $N_{p\text{-pair}}^{\text{eff}}(\mathbf{k})$  grows with  $|V|$ . This directly visualizes the mechanism captured by the projected coupling  $g_{p_x} = g_{p_y} = 2V$  and the channel-resolved Landau analysis: nonlocal attraction activates the equal-spin triplet Cooper channel, while the momentum-space vertex distribution reveals where the enhancement is concentrated.

In contrast, the anisotropy parameter  $\alpha$  primarily regulates the structure and orientation of the  $p$ -wave correlations. At the strong anisotropy  $\alpha = 0.02$ , the weight near  $\Gamma$  is sharply elongated along a single momentum axis [Figs. 4(a)–4(d)], consistent with strongly distorted spin-resolved Fermi surface patches [Fig. 4(e)] that lift the near-degeneracy between the  $p_x$  and  $p_y$  components. For  $\alpha = 0.50$ , the spin-resolved Fermi surface becomes more nearly  $C_4$  symmetric [Fig. 4(j)], and the  $p$ -wave pairing distribution correspondingly evolves toward a more fourfold, quasi-isotropic lobe structure [Figs. 4(f)–4(i)]. Thus, within the regime studied, anisotropy does not primarily amplify the total triplet weight; rather, it selects the polar orientation and reshapes the momentum-space morphology of the  $p$ -wave pairing correlations through Fermi surface deformation.

Taken together, the results establish a coherent microscopic picture for the emergence of an oriented triplet state in the spin-anisotropic attractive  $t-U-V$  Hubbard model. A finite NN attraction is essential to activate an odd-parity Cooper channel, while the spin-dependent hopping anisotropy  $\alpha$  suppresses the competing onsite singlet coherence and, by deforming the spin-resolved Fermi surface, selects a polar axis (either  $p_x$  or  $p_y$ ) for the triplet correlations. This cooperative mechanism explains both the topology of the  $(V, \alpha)$  phase diagram and the strongly anisotropic momentum-space vertex patterns in the  $p$ -TP regime.

In summary, we mapped the ground-state phase diagram of the attractive  $t - U - V$  Hubbard model at  $n \simeq 0.85$ , identified CPBM,  $s$ -SF and  $p$ -TP phases using quantum Monte Carlo simulations. Momentum-resolved vertex distributions and real-space correlators provide distinct signatures: the CPBM exhibits a broad Bose-surface feature without a condensate peak and no off-diagonal long-range order, the  $s$ -SF develops a sharp  $\Gamma$ -point condensate peak, and the  $p$ -TP shows an anisotropically elongated  $p$ -wave weight locked to the spin-split Fermi surface patches. Finally, a channel-resolved Landau analysis yields a compact  $p$ -wave Thouless scale

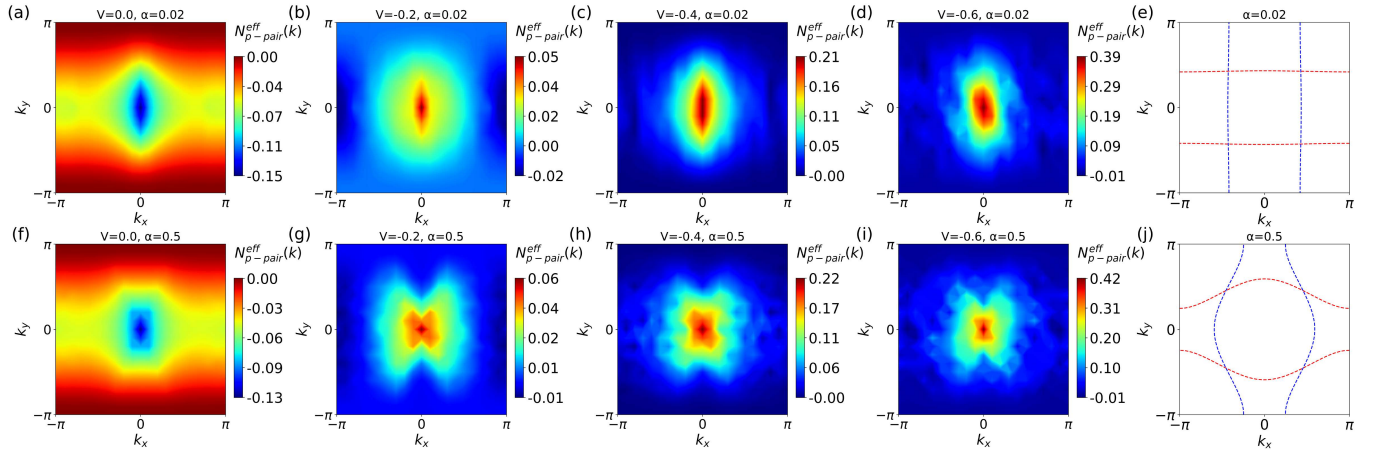


FIG. 4. (Color online) Momentum-space evolution of  $N_{p\text{-pair}}^{\text{eff}}(\mathbf{k})$ . Top row:  $\alpha = 0.02$ . Panels (a)–(d) correspond to  $V = 0, -0.2, -0.4, -0.6$ , and panel (e) shows the associated spin-resolved Fermi surface for  $\uparrow/\downarrow$  (blue/red dashed curves). Bottom row:  $\alpha = 0.50$ . Panels (f)–(i) show the same sequence of  $V$ , and panel (j) displays the corresponding Fermi surface. For  $V = 0$ , the  $p$ -wave signal is absent; increasing  $|V|$  redistributes spectral weight toward  $\Gamma$  and produces oriented lobes signaling the emergence of odd-parity triplet correlations. For stronger anisotropy (smaller  $\alpha$ ), the distribution elongates along a single polar axis ( $p_x$  or  $p_y$ ), indicating that anisotropy selects the orientation of the  $p$ -wave channel via Fermi surface deformation. At fixed  $V$ , the total magnitude of the  $p$ -wave signal remains comparable between the two anisotropies, with only minor numerical variations.

$|V_c^L(\alpha)|$  [Eq. (11)], whose anisotropy dependence tracks the crossover boundary into the triplet dominant regime.

More broadly, the mechanism uncovered here—finite-range attraction opening an odd-parity channel and momentum-space Fermi surface geometry selecting its orientation—should be relevant in other spin-split metals. In particular, altermagnetic band structures exhibit symmetry-enforced momentum-dependent spin polarization without net magnetization, producing spin-resolved Fermi surface patches analogous to those controlling the present instability [49–64]. Therefore, it would be interesting to extend the present microscopic framework to other altermagnetic Hamiltonians with effective attractive interactions, and further identify the finite-momentum paired state.

Z.C. acknowledges support from China Postdoctoral Science Foundation (2025M783397). H.K.T acknowledges support from the Shenzhen Fundamental Research Program (No. JCYJ20250604145655074) and Shenzhen Key Laboratory of Advanced Functional Carbon Materials Research and Comprehensive Application (No. ZDSYS20220527171407017). T.Y. acknowledges support from Natural Science Foundation of Heilongjiang Province (No. YQ2023A004). M.Z. is supported by the National Natural Science Foundation of China under Grant No. 12504172. This work is supported by the Research Foundation of Yanshan University under Grant No. 8190448.

The data are available from the authors upon reasonable request.

---

[1] Q. Gu, S. Wang, J. P. Carroll, K. Zhussupbekov, C. Broyles, S. Ran, N. P. Butch, J. A. Horn, S. Saha, J. Paglione, *et al.*, Pair wave function symmetry in  $\text{UTe}_2$  from zero-energy surface state visualization, *Science* **388**, 938 (2025).

[2] K. Nogaki and Y. Yanase, Even-odd parity transition in strongly correlated locally noncentrosymmetric superconductors: Application to  $\text{CeRh}_2\text{As}_2$ , *Phys. Rev. B* **106**, L100504 (2022).

[3] X. Xu, Y. Li, and C. L. Chien, Observation of odd-parity superconductivity with the geshkenbein–larkin–barone composite rings, *Phys. Rev. Lett.* **132**, 056001 (2024).

[4] J. D. Strand, D. J. Bahr, D. J. Van Harlingen, J. P. Davis, W. J. Gannon, and W. P. Halperin, The transition between real and complex superconducting order parameter phases in  $\text{UPt}_3$ , *Science* **328**, 1368 (2010).

[5] S. Ran, C. Eckberg, Q.-P. Ding, Y. Furukawa, T. Metz, S. R. Saha, I.-L. Liu, M. Zic, H. Kim, J. Paglione, *et al.*, Nearly ferromagnetic spin-triplet superconductivity, *Science* **365**, 684 (2019).

[6] A. J. Leggett, A theoretical description of the new phases of liquid  $^3\text{He}$ , *Rev. Mod. Phys.* **47**, 331 (1975).

[7] A. P. Mackenzie and Y. Maeno, The superconductivity of  $\text{Sr}_2\text{RuO}_4$  and the physics of spin-triplet pairing, *Rev. Mod. Phys.* **75**, 657 (2003).

[8] N. Read and D. Green, Paired states of fermions in two dimensions with breaking of parity and time-reversal symmetries and the fractional quantum hall effect, *Phys. Rev. B* **61**, 10267 (2000).

[9] S. Wolf, T. Gardener, K. Le Hur, and S. Rachel, Topological superconductivity on the honeycomb lattice: Ef-

fect of normal-state topology, *Phys. Rev. B* **105**, L100505 (2022).

[10] S. Wolf, D. Di Sante, T. Schwemmer, R. Thomale, and S. Rachel, Triplet superconductivity from nonlocal coulomb repulsion in an atomic Sn layer deposited onto a Si(111) substrate, *Phys. Rev. Lett.* **128**, 167002 (2022).

[11] J. Alicea, New directions in the pursuit of Majorana fermions in solid state systems, *Rep. Prog. Phys.* **75**, 076501 (2012).

[12] C. W. J. Beenakker, Search for Majorana fermions in superconductors, *Annu. Rev. Condens. Matter Phys.* **4**, 113 (2013).

[13] T. D. Stanescu and S. Tewari, Majorana fermions in semiconductor nanowires: Fundamentals, modeling, and experiment, *J. Phys.: Condens. Matter* **25**, 233201 (2013).

[14] S. R. Elliott and M. Franz, Colloquium: Majorana fermions in nuclear, particle, and solid-state physics, *Rev. Mod. Phys.* **87**, 137 (2015).

[15] A. Y. Kitaev, Unpaired Majorana fermions in quantum wires, *Phys. Usp.* **44**, 131 (2001), arXiv:cond-mat/0010440 [cond-mat.mes-hall].

[16] C. A. Regal, C. Ticknor, J. L. Bohn, and D. S. Jin, Tuning  $p$ -wave interactions in an ultracold Fermi gas of atoms, *Phys. Rev. Lett.* **90**, 053201 (2003).

[17] C. Ticknor, C. A. Regal, D. S. Jin, and J. L. Bohn, Multiplet structure of Feshbach resonances in nonzero partial waves, *Phys. Rev. A* **69**, 042712 (2004).

[18] J. Zhang, E. G. M. van Kempen, T. Bourdel, L. Khaykovich, J. Cubizolles, F. Chevy, M. Teichmann, L. Tarruell, S. J. J. M. F. Kokkelmans, and C. Salomon,  $p$ -wave Feshbach resonances of ultracold  $^6\text{Li}$ , *Phys. Rev. A* **70**, 030702 (2004).

[19] J. Levinsen, N. R. Cooper, and V. Gurarie, Strongly resonant  $p$ -wave superfluids, *Phys. Rev. Lett.* **99**, 210402 (2007).

[20] H. Hu and X.-J. Liu, Resonantly interacting  $p$ -wave fermi superfluid in two dimensions: Tan's contact and the breathing mode, *Phys. Rev. A* **100**, 023611 (2019).

[21] A. E. Feiguin and M. P. A. Fisher, Exotic paired states with anisotropic spin-dependent Fermi surfaces, *Phys. Rev. Lett.* **103**, 025303 (2009).

[22] J. Gukelberger, E. Kozik, L. Pollet, N. Prokof'ev, M. Sigrist, B. Svistunov, and M. Troyer,  $p$ -wave superfluidity by spin-nematic fermi surface deformation, *Phys. Rev. Lett.* **113**, 195301 (2014).

[23] P. Phillips and D. Dalidovich, The elusive Bose metal, *Science* **302**, 243 (2003).

[24] J. Su, J. Liu, J. Li, Z. Cao, T. Ying, and H.-K. Tang, Variation of bose surface by filling in Cooper-pair Bose metal, *Phys. Rev. B* **112**, 174518 (2025).

[25] Z. Cao, J. Su, J. Li, T. Ying, W. Wang, J.-H. Sun, H.-K. Tang, and H.-Q. Lin, Exotic  $d$ -wave cooper-pair Bose metal in two dimensions, *Phys. Rev. B* **110**, 224522 (2024).

[26] S. Nayak, N. Batra, and S. Kumar, Pairing symmetries in the Zeeman-coupled extended attractive Hubbard model, *Sci. Rep.* **11**, 22724 (2021).

[27] D.-W. Qu, B.-B. Chen, H.-C. Jiang, Y. Wang, and W. Li, Spin-triplet pairing induced by near-neighbor attraction in the extended Hubbard model for cuprate chain, *Commun. Phys.* **5**, 257 (2022).

[28] Z. Cao, J. Li, J. Su, T. Ying, and H.-K. Tang, Dominant  $p$ -wave pairing induced by nearest-neighbor attraction in the square-lattice extended Hubbard model, *Phys. Rev. B* **111**, 024509 (2025).

[29] S. Zhang, J. Carlson, and J. E. Gubernatis, Constrained path Monte Carlo method for fermion ground states, *Phys. Rev. B* **55**, 7464 (1997).

[30] S. Zhang, J. Carlson, and J. E. Gubernatis, Constrained path quantum Monte Carlo method for fermion ground states, *Phys. Rev. Lett.* **74**, 3652 (1995).

[31] R. Micnas, J. Ranninger, and S. Robaszkiewicz, Superconductivity in narrow-band systems with local nonretarded attractive interactions, *Rev. Mod. Phys.* **62**, 113 (1990).

[32] M. Randeria, J.-M. Duan, and L.-Y. Shieh, Bound states, cooper pairing, and bose condensation in two dimensions, *Phys. Rev. Lett.* **62**, 981 (1989).

[33] M. Randeria, N. Trivedi, A. Moreo, and R. T. Scalettar, Pairing and spin gap in the normal state of short coherence length superconductors, *Phys. Rev. Lett.* **69**, 2001 (1992), erratum: *Phys. Rev. Lett.* **72**, 3292 (1994).

[34] M. Greiner, C. A. Regal, and D. S. Jin, Emergence of a molecular Bose-Einstein condensate from a fermi gas, *Nature* **426**, 537 (2003).

[35] S. Jochim, M. Bartenstein, A. Altmeyer, G. Hendl, S. Riedl, C. Chin, J. Hecker Denschlag, and R. Grimm, Bose-Einstein condensation of molecules, *Science* **302**, 2101 (2003).

[36] See Supplemental Material, which includes Refs. [? ? ? ? ? ], for details on the method and additional simulation results.

[37] S. R. White, D. J. Scalapino, R. L. Sugar, N. E. Bickers, and R. T. Scalettar, Attractive and repulsive pairing interaction vertices for the two-dimensional Hubbard model, *Phys. Rev. B* **39**, 839 (1989).

[38] T. Ying and S. Wessel, Pairing and chiral spin density wave instabilities on the honeycomb lattice: A comparative quantum Monte Carlo study, *Phys. Rev. B* **97**, 075127 (2018).

[39] A. Einstein, Quantentheorie des einatomigen idealen gases. zweite abhandlung, in *Albert Einstein: Akademie-Vorträge: Sitzungsberichte der Preußischen Akademie der Wissenschaften 1914–1932* (Wiley, 2005) pp. 245–257.

[40] M. H. Anderson, J. R. Ensher, M. R. Matthews, C. E. Wieman, and E. A. Cornell, Observation of Bose-Einstein condensation in a dilute atomic vapor, *Science* **269**, 198 (1995).

[41] A. Altland and B. Simons, *Condensed Matter Field Theory*, 2nd ed. (Cambridge University Press, 2010).

[42] M. Tinkham, *Introduction to Superconductivity*, 2nd ed. (McGraw-Hill, New York, 1996).

[43] D. J. Thouless, Stability conditions and nuclear rotations in the Hartree-Fock theory, *Ann. Phys.* **10**, 553 (1960).

[44] P. Nozières and S. Schmitt-Rink, Bose condensation in an attractive fermion gas: From weak to strong coupling superconductivity, *J. Low Temp. Phys.* **59**, 195 (1985).

[45] Q. Chen, J. Stajic, S. Tan, and K. Levin, BCS-BEC crossover: From high temperature superconductors to ultracold superfluids, *Phys. Rep.* **412**, 1 (2005).

[46] S. Nayak and S. Kumar, Exotic superconducting states in the extended attractive Hubbard model, *J. Phys.: Condens. Matter* **30**, 135601 (2018).

[47] R. Micnas, J. Ranninger, S. Robaszkiewicz, and S. Tabor, Superconductivity in a narrow-band system with intersite electron pairing in two dimensions: A mean-field study, *Phys. Rev. B* **37**, 9410 (1988).

[48] S. Hong, M. J. Park, and K.-M. Kim, Unconventional  $p$ -wave and finite-momentum superconductivity induced by altermagnetism through the formation of Bogoliubov Fermi surface, *Phys. Rev. B* **111**, 054501 (2025).

[49] O. Fedchenko, J. Minár, Akashdeep, S. W. D'Souza, D. Vasilyev, O. Tkach, L. Odenbreit, Q. L. Nguyen, D. Kutnyakhov, N. Wind, L. Wenthaus, M. Scholz, K. Rossnagel, M. Hoesch, M. Aeschlimann, B. Stadtmüller, M. Kläui, G. Schönhense, G. Jakob, T. Jungwirth, L. Šmejkal, J. Sinova, and H.-J. Elmers, Observation of time-reversal symmetry breaking in the band structure of altermagnetic RuO<sub>2</sub>, *Sci. Adv.* **10**, eadj4883 (2024).

[50] J. Krempaský, L. Šmejkal, S. W. D'Souza, M. Hajaoui, G. Springholz, K. Uhlířová, F. Alarab, P. C. Constantinou, V. N. Strocov, D. Usanov, W. R. Pudelko, R. González-Hernández, A. B. Hellenes, Z. Jansa, H. Reichlová, Z. Šobáň, R. D. Gonzalez Betancourt, P. Wadley, J. Sinova, D. Kriegner, J. Minár, J. H. Dil, and T. Jungwirth, Altermagnetic lifting of Kramers spin degeneracy, *Nature* **626**, 517 (2024).

[51] T. Osumi, S. Souma, T. Aoyama, K. Yamauchi, A. Honma, K. Nakayama, T. Takahashi, K. Ohgushi, and T. Sato, Observation of a giant band splitting in altermagnetic MnTe, *Phys. Rev. B* **109**, 115102 (2024).

[52] S. Reimers, L. Odenbreit, L. Šmejkal, V. N. Strocov, P. Constantinou, A. B. Hellenes, R. Jaeschke Ubiergo, W. H. Campos, V. K. Bharadwaj, A. Chakraborty, T. Denneulin, W. Shi, R. E. Dunin-Borkowski, S. Das, M. Kläui, J. Sinova, and M. Jourdan, Direct observation of altermagnetic band splitting in CrSb thin films, *Nat. Commun.* **15**, 2116 (2024).

[53] M. Zeng *et al.*, Observation of spin splitting in room-temperature metallic antiferromagnet CrSb, *Adv. Sci.* **11**, 2406529 (2024).

[54] J. Ding, Z. Jiang, X. Chen, Z. Tao, Z. Liu, J. Liu, T. Li, J. Liu, Y. Yang, R. Zhang, L. Deng, W. Jing, Y. Huang, Y. Shi, S. Qiao, Y. Wang, Y. Guo, D. Feng, and D. Shen, Large band-splitting in  $g$ -wave type altermagnet CrSb, *Phys. Rev. Lett.* **133**, 206401 (2024).

[55] Y. Noda, K. Ohno, and S. Nakamura, Momentum-dependent band spin splitting in semiconducting MnO<sub>2</sub>: A density functional calculation, *Phys. Chem. Chem. Phys.* **18**, 13294 (2016).

[56] L. Šmejkal, R. González-Hernández, T. Jungwirth, and J. Sinova, Crystal time-reversal symmetry breaking and spontaneous hall effect in collinear antiferromagnets, *Sci. Adv.* **6**, eaaz8809 (2020).

[57] S. Hayami, Y. Yanagi, and H. Kusunose, Momentum-dependent spin splitting by collinear antiferromagnetic ordering, *J. Phys. Soc. Jpn.* **88**, 123702 (2019).

[58] K.-H. Ahn, A. Hariki, K.-W. Lee, and J. Kuneš, Antiferromagnetism in RuO<sub>2</sub> as  $d$ -wave Pomeranchuk instability, *Phys. Rev. B* **99**, 184432 (2019).

[59] L.-D. Yuan, Z. Wang, J.-W. Luo, E. I. Rashba, and A. Zunger, Giant momentum-dependent spin splitting in centrosymmetric low- $Z$  antiferromagnets, *Phys. Rev. B* **102**, 014422 (2020).

[60] L.-D. Yuan, Z. Wang, J.-W. Luo, and A. Zunger, Prediction of low- $Z$  collinear and noncollinear antiferromagnetic compounds having momentum-dependent spin splitting even without spin-orbit coupling, *Phys. Rev. Mater.* **5**, 014409 (2021).

[61] L. Šmejkal, J. Sinova, and T. Jungwirth, Emerging research landscape of altermagnetism, *Phys. Rev. X* **12**, 040501 (2022).

[62] L. Šmejkal, J. Sinova, and T. Jungwirth, Beyond conventional ferromagnetism and antiferromagnetism: A phase with nonrelativistic spin and crystal rotation symmetry, *Phys. Rev. X* **12**, 031042 (2022).

[63] I. Mazin and T. P. Editors, Editorial: Altermagnetism—a new punch line of fundamental magnetism, *Phys. Rev. X* **12**, 040002 (2022).

[64] L. Bai, W. Feng, S. Liu, L. Šmejkal, Y. Mokrousov, and Y. Yao, Altermagnetism: Exploring new frontiers in magnetism and spintronics, *Adv. Funct. Mater.* **34**, 2409327 (2024).

# Supplemental Material for “Oriented Triplet $p$ -Wave Pairing from Fermi surface Anisotropy and Nonlocal Attraction”

Shuning Tan,<sup>1,\*</sup> Ji Liu,<sup>2,3,\*</sup> Minghuan Zeng,<sup>4</sup> Tao Ying,<sup>5</sup> Zhangkai Cao,<sup>6,7,†</sup> and Ho-Kin Tang<sup>2,3,‡</sup>

<sup>1</sup>*Key Laboratory for Microstructural Material Physics of Hebei Province,  
School of Science, Yanshan University, Qinhuangdao 066004, China*

<sup>2</sup>*School of Science, Harbin Institute of Technology, Shenzhen, 518055, China*

<sup>3</sup>*Shenzhen Key Laboratory of Advanced Functional Carbon Materials  
Research and Comprehensive Application, Shenzhen 518055, China.*

<sup>4</sup>*College of Physics, Chongqing University, Chongqing 401331, China*

<sup>5</sup>*School of Physics, Harbin Institute of Technology, Harbin 150001, China*

<sup>6</sup>*Eastern Institute for Advanced Study, Eastern Institute of Technology, Ningbo, Zhejiang 315200, China*

<sup>7</sup>*School of Physical Sciences, University of Science and Technology of China, Hefei, 230026, China*

(Dated: January 19, 2026)

In this Supplemental Material, we provide additional analytical details and numerical results supporting the main text. In Sec. S1, we derive the quadratic Landau coefficients used in Eqs.(6)–(11) of the main text by projecting the microscopic interactions onto symmetry-adapted pairing channels and evaluating the corresponding normal-state pairing susceptibilities. We also present CPQMC momentum-resolved vertex distributions for the extended- $s'$  and  $d_{x^2-y^2}$  channels to confirm that they remain subleading in the parameter regime studied. In Sec. S2, we provide additional CPQMC results for the momentum-resolved effective  $s$ - and  $p$ -wave pair distributions  $N_\ell^{\text{eff}}(\mathbf{k})$ , illustrating the anisotropy-driven evolution across the  $s$ -SF, CPBM, and  $p$ -TP regimes.

## S1. Mean-field origin of the Landau coefficients

For completeness, we outline the minimal steps leading from the microscopic interactions to the quadratic Landau coefficients quoted in the main text.

### A. Projection of the microscopic interactions

For later convenience, we rewrite the spin-anisotropic attractive  $t-U-V$  Hubbard model of Eq. (1) of the main text in momentum space and separate it into a quadratic part and an interaction part,

$$\hat{H} = \hat{H}_0 + \hat{H}_{\text{int}}, \quad (\text{S1})$$

with

$$\hat{H}_0 = \sum_{\mathbf{k},\sigma} \xi_{\mathbf{k}\sigma} \hat{c}_{\mathbf{k}\sigma}^\dagger \hat{c}_{\mathbf{k}\sigma}, \quad (\text{S2})$$

$$\hat{H}_{\text{int}} = \frac{1}{N} \sum_{\mathbf{k},\mathbf{k}'} \sum_{\sigma,\sigma'} V(\mathbf{k}, \mathbf{k}') \hat{c}_{\mathbf{k}\sigma}^\dagger \hat{c}_{-\mathbf{k}\sigma'}^\dagger \hat{c}_{-\mathbf{k}'\sigma'} \hat{c}_{\mathbf{k}'\sigma}. \quad (\text{S3})$$

Here  $\xi_{\mathbf{k}\sigma}$  is the spin-dependent anisotropic dispersion given in the main text, and  $V(\mathbf{k}, \mathbf{k}')$  is the interaction kernel defined in Eq. (6). Throughout we focus on uniform pairing instabilities and hence restrict to the zero center-of-mass ( $\mathbf{q} = 0$ ) Cooper channel.

Introducing the symmetry-adapted basis functions

$$\begin{aligned} \phi_s(\mathbf{k}) &= 1, & \phi_{s'}(\mathbf{k}) &= \frac{1}{2} (\cos k_x + \cos k_y), & \phi_{d_{x^2-y^2}}(\mathbf{k}) &= \frac{1}{2} (\cos k_x - \cos k_y), \\ \phi_{p_x}(\mathbf{k}) &= \sin k_x, & \phi_{p_y}(\mathbf{k}) &= \sin k_y. \end{aligned} \quad (\text{S4})$$

\* These authors contributed equally.

† [caozhangkai@mail.bnu.edu.cn](mailto:caozhangkai@mail.bnu.edu.cn)

‡ [denghaojian@hit.edu.cn](mailto:denghaojian@hit.edu.cn)

projecting  $V(\mathbf{k}, \mathbf{k}')$  onto these channels yields the bare channel couplings

$$g_s = U, \quad g_{s'} = 4V, \quad g_{d_{x^2-y^2}} = 4V, \quad g_{p_x} = g_{p_y} = 2V. \quad (\text{S5})$$

For  $U < 0$  and  $V < 0$ , the channel couplings  $g_\ell$  are negative. It is therefore convenient to introduce the attraction strengths  $|g_\ell| \equiv -g_\ell > 0$  and write the interaction projected onto the symmetry-adapted Cooper channels in separable form,

$$\begin{aligned} \hat{H}_{\text{int}} = & - \sum_{\ell \in \{s, s', d_{x^2-y^2}\}} \frac{|g_\ell|}{N} \sum_{\mathbf{k}, \mathbf{k}'} \phi_\ell(\mathbf{k}) \phi_\ell(\mathbf{k}') \hat{c}_{\mathbf{k}\uparrow}^\dagger \hat{c}_{-\mathbf{k}\downarrow}^\dagger \hat{c}_{-\mathbf{k}'\downarrow} \hat{c}_{\mathbf{k}'\uparrow} \\ & - \sum_{\eta=x, y} \sum_{\sigma=\uparrow, \downarrow} \frac{|g_{p_\eta}|}{N} \sum_{\mathbf{k}, \mathbf{k}'} \phi_{p_\eta}(\mathbf{k}) \phi_{p_\eta}(\mathbf{k}') \hat{c}_{\mathbf{k}\sigma}^\dagger \hat{c}_{-\mathbf{k}\sigma}^\dagger \hat{c}_{-\mathbf{k}'\sigma} \hat{c}_{\mathbf{k}'\sigma}. \end{aligned} \quad (\text{S6})$$

Although the NN attraction generates identical bare couplings  $g_{s'} = g_{d_{x^2-y^2}} = 4V$  in the extended- $s'$  and  $d_{x^2-y^2}$  channels, their impact on pairing is controlled by the corresponding susceptibilities. As a consistency check, we compute the momentum-resolved effective pairing weights in these channels using CPQMC (see Figs. S1 and S2), which confirms that the extended- $s'$  and  $d_{x^2-y^2}$  channels remain subleading in the parameter regime of interest.

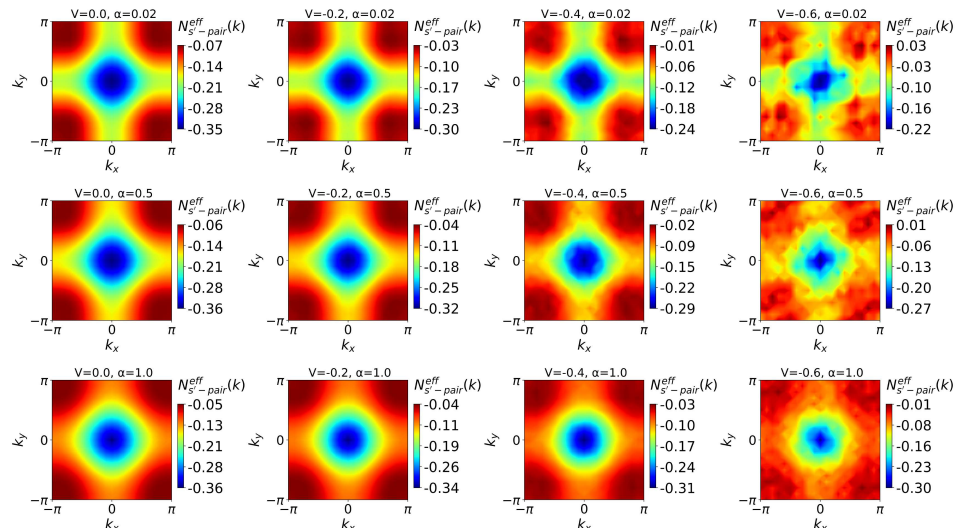


FIG. S1. (Color online) CPQMC results for the effective extended- $s$ -wave pair momentum distribution  $N_{s'-\text{pair}}^{\text{eff}}(\mathbf{k})$  on a  $20 \times 20$  lattice at filling  $n \simeq 0.85$ , shown for several values of the nearest-neighbor attraction  $V$  and hopping anisotropy  $\alpha$ . Although the extended- $s$  channel is symmetry-allowed by the NN attraction, its overall magnitude remains small and no sharp condensation features develop, indicating that this channel is subleading throughout the parameter regime studied.

## B. Grassmann path-integral representation

We start from the partition function  $Z = \text{Tr } e^{-\beta H}$  and use fermionic coherent states to write it as a Grassmann path integral [S1–S6],

$$Z = \int \mathcal{D}[\bar{\psi}, \psi] e^{-S[\bar{\psi}, \psi]}, \quad (\text{S7})$$

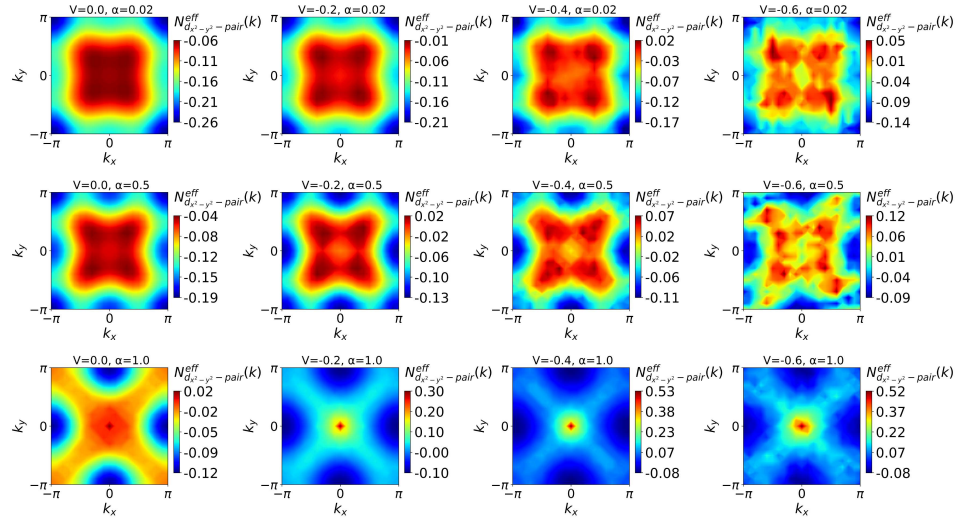


FIG. S2. (Color online) CPQMC results for the effective  $d_{x^2-y^2}$ -wave pair momentum distribution  $N_{d_{x^2-y^2}-\text{pair}}^{\text{eff}}(\mathbf{k})$  on a  $20 \times 20$  lattice at filling  $n \simeq 0.85$ , for the same set of parameters as in Fig. S1. Despite the presence of a finite projected coupling  $g_{d_{x^2-y^2}} = 4V$ , the  $d$ -wave channel remains weak and does not exhibit a dominant pairing instability, consistent with the channel-resolved Landau analysis

with the Euclidean action

$$S[\bar{\psi}, \psi] = \int_0^\beta d\tau \left[ \sum_{\mathbf{k}, \sigma} \bar{\psi}_{\mathbf{k}\sigma}(\tau) (\partial_\tau + \xi_{\mathbf{k}\sigma}) \psi_{\mathbf{k}\sigma}(\tau) - \sum_{\ell \in \{s, s', d_{x^2-y^2}\}} \frac{|g_\ell|}{N} \sum_{\mathbf{k}, \mathbf{k}'} \phi_\ell(\mathbf{k}) \phi_\ell(\mathbf{k}') \bar{\psi}_{\mathbf{k}\uparrow}(\tau) \bar{\psi}_{-\mathbf{k}\downarrow}(\tau) \psi_{-\mathbf{k}'\downarrow}(\tau) \psi_{\mathbf{k}'\uparrow}(\tau) - \sum_{\eta=x, y} \sum_{\sigma=\uparrow, \downarrow} \frac{|g_{p_\eta}|}{N} \sum_{\mathbf{k}, \mathbf{k}'} \phi_{p_\eta}(\mathbf{k}) \phi_{p_\eta}(\mathbf{k}') \bar{\psi}_{\mathbf{k}\sigma}(\tau) \bar{\psi}_{-\mathbf{k}\sigma}(\tau) \psi_{-\mathbf{k}'\sigma}(\tau) \psi_{\mathbf{k}'\sigma}(\tau) \right]. \quad (\text{S8})$$

Here  $\bar{\psi}_{\mathbf{k}\sigma}(\tau)$  and  $\psi_{\mathbf{k}\sigma}(\tau)$  are Grassmann fields,  $\beta = 1/T$ . The form factors  $\phi_\ell(\mathbf{k})$  are defined in Eq. S4. We restrict to uniform ( $\mathbf{q} = 0$ ) pairing instabilities and thus keep only the zero-momentum Cooper channel.

### C. Hubbard–Stratonovich decoupling in pairing channels

The quartic interactions in the projected ( $\mathbf{q} = 0$ ) Cooper channels can be decoupled by introducing complex Hubbard–Stratonovich (HS) pairing fields [S1–S6]. This HS transformation is an *exact* identity; a mean-field approximation is invoked only if one subsequently evaluates the HS functional integral at a saddle point.

In this work we keep only the on-site singlet  $s$  channel and the nearest-neighbor (NN) equal-spin triplet  $p$  channels. The corresponding separable form factors are  $\phi_s(\mathbf{k}) = 1$  and  $\phi_{p\eta}(\mathbf{k}) = \sin k_\eta$  with  $\eta = x, y$  (so that  $\phi_{p\eta}(-\mathbf{k}) = -\phi_{p\eta}(\mathbf{k})$ , ensuring the required antisymmetry for equal-spin pairing). The attraction strengths are  $|g_s| = |U|$  and  $|g_p| = 2|V|$ .

*Singlet  $s$  channel.* The on-site Cooper interaction can be written as

$$\exp \left[ \frac{|U|}{N} \int_0^\beta d\tau \sum_{\mathbf{k}, \mathbf{k}'} \bar{\psi}_{\mathbf{k}\uparrow}(\tau) \bar{\psi}_{-\mathbf{k}\downarrow}(\tau) \psi_{-\mathbf{k}'\downarrow}(\tau) \psi_{\mathbf{k}'\uparrow}(\tau) \right] \propto \int \mathcal{D}[\Delta_s, \Delta_s^*] e^{-S_{\text{HS}}^{(s)}}, \quad (\text{S9})$$

with

$$S_{\text{HS}}^{(s)} = \int_0^\beta d\tau \left[ \frac{|\Delta_s(\tau)|^2}{|U|} - \frac{\Delta_s(\tau)}{\sqrt{N}} \sum_{\mathbf{k}} \bar{\psi}_{\mathbf{k}\uparrow}(\tau) \bar{\psi}_{-\mathbf{k}\downarrow}(\tau) - \frac{\Delta_s^*(\tau)}{\sqrt{N}} \sum_{\mathbf{k}} \psi_{-\mathbf{k}\downarrow}(\tau) \psi_{\mathbf{k}\uparrow}(\tau) \right]. \quad (\text{S10})$$

*Equal-spin triplet p channels.* Similarly, for each  $(\eta, \sigma)$  with  $\eta = x, y$  and  $\sigma = \uparrow, \downarrow$ , the projected NN Cooper interaction reads

$$\exp \left[ \frac{2|V|}{N} \int_0^\beta d\tau \sum_{\mathbf{k}, \mathbf{k}'} \phi_{p\eta}(\mathbf{k}) \phi_{p\eta}(\mathbf{k}') \bar{\psi}_{\mathbf{k}\sigma}(\tau) \bar{\psi}_{-\mathbf{k}\sigma}(\tau) \psi_{-\mathbf{k}'\sigma}(\tau) \psi_{\mathbf{k}'\sigma}(\tau) \right] \propto \int \mathcal{D}[\Delta_{p\eta, \sigma}, \Delta_{p\eta, \sigma}^*] e^{-S_{\text{HS}}^{(p)}}, \quad (\text{S11})$$

where

$$S_{\text{HS}}^{(p)} = \int_0^\beta d\tau \left[ \frac{|\Delta_{p\eta, \sigma}(\tau)|^2}{2|V|} - \frac{\Delta_{p\eta, \sigma}(\tau)}{\sqrt{N}} \sum_{\mathbf{k}} \phi_{p\eta}(\mathbf{k}) \bar{\psi}_{\mathbf{k}\sigma}(\tau) \bar{\psi}_{-\mathbf{k}\sigma}(\tau) - \frac{\Delta_{p\eta, \sigma}^*(\tau)}{\sqrt{N}} \sum_{\mathbf{k}} \phi_{p\eta}(\mathbf{k}) \psi_{-\mathbf{k}\sigma}(\tau) \psi_{\mathbf{k}\sigma}(\tau) \right]. \quad (\text{S12})$$

*Quadratic fermionic action.* After decoupling the  $s$  and all equal-spin  $p$  channels, the partition function becomes

$$Z = \int \mathcal{D}[\Delta_s, \Delta_s^*] \prod_{\eta=x, y} \prod_{\sigma=\uparrow, \downarrow} \mathcal{D}[\Delta_{p\eta, \sigma}, \Delta_{p\eta, \sigma}^*] \int \mathcal{D}[\bar{\psi}, \psi] \exp \left[ -S_{\text{quad}}[\bar{\psi}, \psi; \Delta] \right], \quad (\text{S13})$$

with the explicit quadratic action

$$S_{\text{quad}}[\bar{\psi}, \psi; \Delta] = \int_0^\beta d\tau \left\{ \sum_{\mathbf{k}, \sigma} \bar{\psi}_{\mathbf{k}\sigma}(\tau) (\partial_\tau + \xi_{\mathbf{k}\sigma}) \psi_{\mathbf{k}\sigma}(\tau) + \frac{|\Delta_s(\tau)|^2}{|U|} + \sum_{\eta, \sigma} \frac{|\Delta_{p\eta, \sigma}(\tau)|^2}{2|V|} \right. \\ \left. - \frac{1}{\sqrt{N}} \sum_{\mathbf{k}} \left[ \Delta_s(\tau) \bar{\psi}_{\mathbf{k}\uparrow}(\tau) \bar{\psi}_{-\mathbf{k}\downarrow}(\tau) + \Delta_s^*(\tau) \psi_{-\mathbf{k}\downarrow}(\tau) \psi_{\mathbf{k}\uparrow}(\tau) \right] \right. \\ \left. - \frac{1}{\sqrt{N}} \sum_{\eta, \sigma} \sum_{\mathbf{k}} \phi_{p\eta}(\mathbf{k}) \left[ \Delta_{p\eta, \sigma}(\tau) \bar{\psi}_{\mathbf{k}\sigma}(\tau) \bar{\psi}_{-\mathbf{k}\sigma}(\tau) + \Delta_{p\eta, \sigma}^*(\tau) \psi_{-\mathbf{k}\sigma}(\tau) \psi_{\mathbf{k}\sigma}(\tau) \right] \right\}. \quad (\text{S14})$$

For the Gaussian (Landau) expansion discussed in the main text, it is sufficient to consider static, uniform HS fields  $\Delta_s(\tau) \equiv \Delta_s$  and  $\Delta_{p\eta, \sigma}(\tau) \equiv \Delta_{p\eta, \sigma}$ .

#### D. Integrating out fermions and Landau expansion via $G_0 + \Sigma_\Delta$

After the Hubbard–Stratonovich (HS) decoupling in the  $s$ -wave singlet channel and the NN equal-spin  $p$ -wave channels, the fermionic action is quadratic in the Grassmann fields. Restricting to uniform ( $\mathbf{q} = 0$ ) and static HS fields,  $\Delta_s(\tau) = \Delta_s$  and  $\Delta_{p\eta, \sigma}(\tau) = \Delta_{p\eta, \sigma}$ , the partition function takes the form

$$Z = \int \mathcal{D}[\Delta, \Delta^*] e^{-S_B[\Delta, \Delta^*]} \int \mathcal{D}[\bar{\psi}, \psi] e^{-S_F[\bar{\psi}, \psi; \Delta, \Delta^*]}, \quad (\text{S15})$$

with the bosonic (HS) weight

$$S_B[\Delta, \Delta^*] = \beta \left( \frac{|\Delta_s|^2}{|U|} + \sum_{\eta=x, y} \sum_{\sigma=\uparrow, \downarrow} \frac{|\Delta_{p\eta, \sigma}|^2}{2|V|} \right), \quad (\text{S16})$$

and  $\beta = 1/T$ .

*a. Nambu representation and anomalous self-energy.* It is convenient to write the quadratic fermionic action in Nambu space. We define the four-component Nambu spinor

$$\Psi_{\mathbf{k}, n} \equiv \begin{pmatrix} \psi_{\mathbf{k}\uparrow}(i\omega_n) \\ \psi_{\mathbf{k}\downarrow}(i\omega_n) \\ \bar{\psi}_{-\mathbf{k}\uparrow}(-i\omega_n) \\ \bar{\psi}_{-\mathbf{k}\downarrow}(-i\omega_n) \end{pmatrix}, \quad \omega_n = (2n+1)\pi T, \quad (\text{S17})$$

so that

$$S_F = \frac{1}{2} \sum_{\mathbf{k}, n} \bar{\Psi}_{\mathbf{k}, n} [\mathcal{G}_0^{-1}(\mathbf{k}, i\omega_n) - \Sigma_\Delta(\mathbf{k})] \Psi_{\mathbf{k}, n}. \quad (\text{S18})$$

Here the normal-state (free) Nambu Green's function is block diagonal,

$$\mathcal{G}_0^{-1}(\mathbf{k}, i\omega_n) = \begin{pmatrix} i\omega_n - \xi_{\mathbf{k}\uparrow} & 0 & 0 & 0 \\ 0 & i\omega_n - \xi_{\mathbf{k}\downarrow} & 0 & 0 \\ 0 & 0 & i\omega_n + \xi_{\mathbf{k}\uparrow} & 0 \\ 0 & 0 & 0 & i\omega_n + \xi_{\mathbf{k}\downarrow} \end{pmatrix}, \quad (\text{S19})$$

with  $\xi_{\mathbf{k}\sigma}$  given in the main text.

The HS pairing fields generate an off-diagonal (anomalous) self-energy

$$\Sigma_{\Delta}(\mathbf{k}) = \begin{pmatrix} 0 & \hat{\Delta}(\mathbf{k}) \\ \hat{\Delta}^{\dagger}(\mathbf{k}) & 0 \end{pmatrix}, \quad (\text{S20})$$

where the  $2 \times 2$  gap matrix in spin space is

$$\hat{\Delta}(\mathbf{k}) = \begin{pmatrix} \Delta_{\uparrow\uparrow}(\mathbf{k}) & \Delta_s \\ -\Delta_s & \Delta_{\downarrow\downarrow}(\mathbf{k}) \end{pmatrix}. \quad (\text{S21})$$

In our channel restriction,

$$\Delta_{\sigma\sigma}(\mathbf{k}) = \sum_{\eta=x,y} \Delta_{p\eta,\sigma} \phi_{p\eta}(\mathbf{k}), \quad \phi_{p\eta}(\mathbf{k}) = \sin k_{\eta}, \quad (\text{S22})$$

and the odd parity  $\phi_{p\eta}(-\mathbf{k}) = -\phi_{p\eta}(\mathbf{k})$  ensures the antisymmetry of equal-spin pairing. (For on-site  $s$  wave we have  $\phi_s(\mathbf{k}) \equiv 1$ .)

b. *Integrating out fermions.* Using the standard Gaussian Grassmann integral  $\int \mathcal{D}[\bar{\psi}, \psi] \exp[-\bar{\psi} A \psi] = \det A$ , Eq. (S18) yields (up to an irrelevant constant from Nambu doubling)

$$\int \mathcal{D}[\bar{\psi}, \psi] e^{-S_F} \propto \exp \left[ -\frac{1}{2} \text{Tr} \ln (\mathcal{G}_0^{-1} - \Sigma_{\Delta}) \right], \quad (\text{S23})$$

where Tr denotes a trace over momentum, Matsubara frequency, and internal Nambu/spin indices. Therefore the effective action for the HS fields is

$$S_{\text{eff}}[\Delta, \Delta^*] = S_B[\Delta, \Delta^*] - \frac{1}{2} \text{Tr} \ln [\mathcal{G}_0^{-1} - \Sigma_{\Delta}]. \quad (\text{S24})$$

c. *Landau expansion to quadratic order.* To obtain the quadratic Landau coefficients, we expand Eq. (S24) around the normal state:

$$\begin{aligned} -\text{Tr} \ln (\mathcal{G}_0^{-1} - \Sigma_{\Delta}) &= -\text{Tr} \ln \mathcal{G}_0^{-1} - \text{Tr} \ln [\mathcal{G}_0^{-1} - \mathcal{G}_0 \Sigma_{\Delta}] \\ &= -\text{Tr} \ln \mathcal{G}_0^{-1} + \sum_{m=1}^{\infty} \frac{1}{m} \text{Tr} [(\mathcal{G}_0 \Sigma_{\Delta})^m]. \end{aligned} \quad (\text{S25})$$

The linear term ( $m = 1$ ) vanishes because  $\Sigma_{\Delta}$  is purely off-diagonal in Nambu space and the normal state has no anomalous expectation value. Keeping only  $m = 2$  gives

$$S_{\text{eff}}^{(2)} = \beta a_s(T, \alpha) |\Delta_s|^2 + \beta \sum_{\eta, \sigma} a_{p\eta, \sigma}(T, \alpha) |\Delta_{p\eta, \sigma}|^2, \quad (\text{S26})$$

with

$$a_s(T, \alpha) = \frac{1}{|U|} - \Pi_s(T, \alpha), \quad (\text{S27})$$

$$a_{p\eta, \sigma}(T, \alpha) = \frac{1}{2|V|} - \Pi_{p\eta, \sigma}(T, \alpha). \quad (\text{S28})$$

Evaluating the trace in Eq. (S25) at  $m = 2$  leads to the usual Cooper-channel bubbles (computed solely from the free Green's functions  $G_{0,\sigma}(\mathbf{k}, i\omega_n) = (i\omega_n - \xi_{\mathbf{k}\sigma})^{-1}$ ):

$$\Pi_s(T, \alpha) = \frac{1}{\beta N} \sum_{\mathbf{k}, n} G_{0,\uparrow}(\mathbf{k}, i\omega_n) G_{0,\downarrow}(-\mathbf{k}, -i\omega_n), \quad (\text{S29})$$

$$\Pi_{p\eta, \sigma}(T, \alpha) = \frac{1}{\beta N} \sum_{\mathbf{k}, n} \phi_{p\eta}^2(\mathbf{k}) G_{0,\sigma}(\mathbf{k}, i\omega_n) G_{0,\sigma}(-\mathbf{k}, -i\omega_n). \quad (\text{S30})$$

### E. Explicit bubble expressions

Here we perform the Matsubara-frequency summation for the normal-state Cooper bubbles entering the quadratic (Gaussian) Landau coefficients derived in Sec. S1D. Using the free Green's function  $G_{0,\sigma}(\mathbf{k}, i\omega_n) = (i\omega_n - \xi_{\mathbf{k}\sigma})^{-1}$  with  $\omega_n = (2n + 1)\pi T$ , and the even-in-momentum dispersion  $\xi_{-\mathbf{k}\sigma} = \xi_{\mathbf{k}\sigma}$ , we obtain the standard identity

$$\begin{aligned} T \sum_{\omega_n} G_{0,\sigma}(\mathbf{k}, i\omega_n) G_{0,\sigma'}(-\mathbf{k}, -i\omega_n) &= T \sum_{\omega_n} \frac{1}{(i\omega_n - \xi_{\mathbf{k}\sigma})(-i\omega_n - \xi_{\mathbf{k}\sigma'})} \\ &= \frac{1 - n_F(\xi_{\mathbf{k}\sigma}) - n_F(\xi_{\mathbf{k}\sigma'})}{\xi_{\mathbf{k}\sigma} + \xi_{\mathbf{k}\sigma'}} \\ &= \frac{\tanh(\xi_{\mathbf{k}\sigma}/2T) + \tanh(\xi_{\mathbf{k}\sigma'}/2T)}{2(\xi_{\mathbf{k}\sigma} + \xi_{\mathbf{k}\sigma'})}, \end{aligned} \quad (\text{S31})$$

where  $n_F(x) = 1/(e^{x/T} + 1)$  is the Fermi function.

Inserting Eq. (S31) into the channel-resolved bubbles gives the explicit susceptibilities used in the main text. For the on-site singlet  $s$  channel,  $\phi_s(\mathbf{k}) = 1$  and  $(\sigma, \sigma') = (\uparrow, \downarrow)$ ,

$$\Pi_s(T, \alpha) = \frac{1}{N} \sum_{\mathbf{k}} \frac{\tanh(\xi_{\mathbf{k}\uparrow}/2T) + \tanh(\xi_{\mathbf{k}\downarrow}/2T)}{2(\xi_{\mathbf{k}\uparrow} + \xi_{\mathbf{k}\downarrow})}. \quad (\text{S32})$$

For the equal-spin nearest-neighbor  $p_\eta$  channels with  $\phi_{p_\eta}(\mathbf{k}) = \sin k_\eta$  and  $\sigma' = \sigma$ , we obtain

$$\Pi_{p\eta,\sigma}(T, \alpha) = \frac{1}{N} \sum_{\mathbf{k}} \sin^2 k_\eta \frac{\tanh(\xi_{\mathbf{k}\sigma}/2T)}{2\xi_{\mathbf{k}\sigma}}, \quad \eta = x, y, \sigma = \uparrow, \downarrow. \quad (\text{S33})$$

Equations (S32)–(S33) reproduce the explicit bubbles quoted in the main text.

## S2. Anisotropy dependence of effective $s$ - and $p$ -wave pair distributions

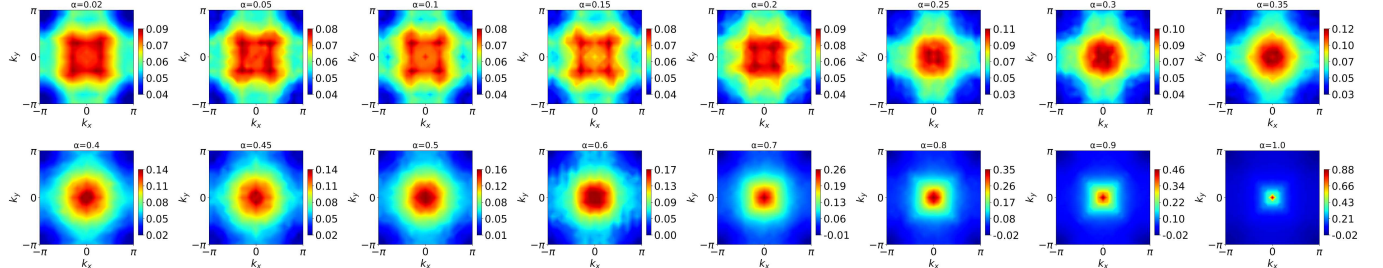


FIG. S3. (Color online) CPQMC results for the effective on-site  $s$ -wave pair momentum distribution  $N_{s\text{-pair}}^{\text{eff}}(\mathbf{k})$  along the representative cut  $V = -0.2$  at filling  $n \simeq 0.85$  on a  $20 \times 20$  lattice, shown for anisotropies  $0.02 \leq \alpha \leq 1$ . The evolution from a broad Bose-surface feature at strong anisotropy (small  $\alpha$ ) to a sharp peak at  $\Gamma$  as  $\alpha \rightarrow 1$  visualizes the crossover from CPBM-like correlations to  $s$ -wave phase coherence.

In this section we examine how the momentum-resolved effective pair distributions  $N_{s\text{-pair}}^{\text{eff}}(\mathbf{k})$  and  $N_{p\text{-pair}}^{\text{eff}}(\mathbf{k})$  respond to the hopping anisotropy  $\alpha$ . All data are obtained from CPQMC simulations at filling  $n \simeq 0.85$  on a  $20 \times 20$  lattice for the representative cut  $V = -0.2$ .

Figure S3 shows  $N_{s\text{-pair}}^{\text{eff}}(\mathbf{k})$  for a sequence of anisotropies  $0.02 \leq \alpha \leq 1$ . In the strong-anisotropy limit (small  $\alpha$ ), the distribution exhibits a broad, nearly square-shaped Bose surface without a sharp condensation peak at  $\Gamma$ , consistent with the CPBM regime. As  $\alpha$  increases (i.e., the anisotropy is reduced), the Bose-surface feature gradually contracts and the weight near  $\Gamma$  is enhanced. Approaching the isotropic limit  $\alpha \rightarrow 1$ ,  $N_{s\text{-pair}}^{\text{eff}}(\mathbf{k})$  develops a pronounced peak at  $\Gamma$ , indicating condensation of Cooper pairs and the onset of long-range  $s$ -wave phase coherence. Conversely, reducing  $\alpha$  suppresses the condensate peak and drives the system into the CPBM regime, consistent with the evolution of the phase boundary in the main-text phase diagram.

Figure S4 displays the corresponding  $p$ -wave vertex distribution  $N_{p\text{-pair}}^{\text{eff}}(\mathbf{k})$  along the same cut  $V = -0.2$ . In contrast to the  $s$ -wave case, the overall magnitude of the  $p$ -wave signal varies only moderately with  $\alpha$ , while its

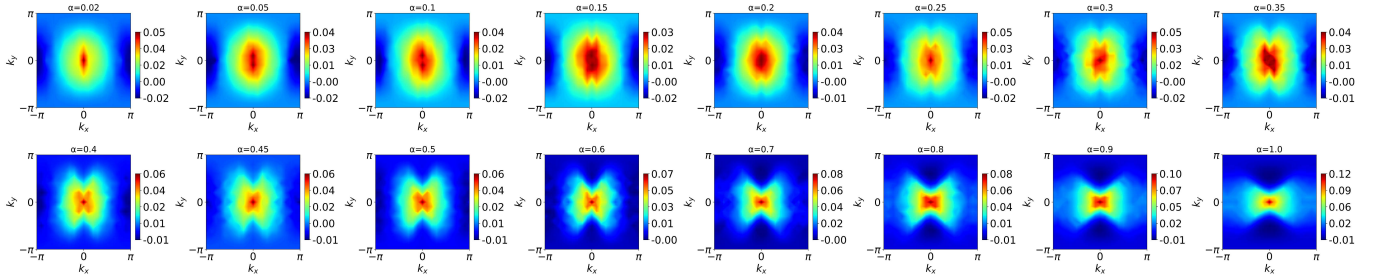


FIG. S4. (Color online) Same as Fig. S3, but for the  $p$ -wave vertex distribution  $N_{p\text{-pair}}^{\text{eff}}(\mathbf{k})$  along the same cut  $V = -0.2$ . While the overall magnitude changes only weakly with  $\alpha$ , strong anisotropy selects a preferred momentum-axis orientation (polar axis) for the  $p$ -wave correlations, and the distribution gradually approaches a more fourfold-symmetric pattern as  $\alpha \rightarrow 1$ .

momentum-space structure is strongly reshaped. For small  $\alpha$ , the distribution forms an elongated feature along a single momentum axis, reflecting that spin-dependent hopping anisotropy lifts the near-degeneracy between the  $p_x$  and  $p_y$  channels and selects a preferred orientation (a polar axis) for triplet correlations. With increasing  $\alpha$ , this anisotropic feature broadens and evolves toward a more fourfold-symmetric pattern, consistent with the reduced spin-dependent Fermi-surface deformation as  $\alpha \rightarrow 1$ . Overall, these results support the main-text conclusion that hopping anisotropy primarily suppresses on-site  $s$ -wave coherence and controls the orientation/morphology of  $p$ -wave correlations, rather than simply amplifying their total weight.

---

[S1] M. Sigrist and K. Ueda, Phenomenological theory of unconventional superconductivity, *Rev. Mod. Phys.* **63**, 239 (1991).  
 [S2] V. P. Mineev and K. V. Samokhin, *Introduction to Unconventional Superconductivity* (Gordon and Breach Science Publishers, Amsterdam, 1999).  
 [S3] K. V. Samokhin, Ginzburg–Landau energy of multiband superconductors with interband pairing, *Phys. Rev. B* **109**, 134508 (2024).  
 [S4] E. I. Blount, Symmetry properties of triplet superconductors, *Phys. Rev. B* **32**, 2935 (1985).  
 [S5] A. Dalal, J. Ruhman, and V. Kozii, Field theory of a superconductor with repulsion, *Phys. Rev. B* **108**, 214521 (2023).  
 [S6] C. Honerkamp and W. Hofstetter, BCS pairing in fermi systems with  $N$  different hyperfine states, *Phys. Rev. B* **70**, 094521 (2004).